scientific reports

Check for updates

OPEN

Neuroprotective effect of intraperitoneal Humanin-G in retinal degeneration of Royal College of Surgeons rats

Bin Lin[1,2,3,4], Kevin Schneider[2,4], Mustafa Ozgul[2], Narcisa Ianopol[2] & Magdalene J. Seiler[1,2,3]✉

This study aimed to examine whether Humanin-G (HNG), a mitochondrial derived peptide with cytoprotective properties, could improve the retinal function and gene expression in Royal College of Surgeons (RCS) rats with retinal pigment epithelium (RPE) dysfunction and retinal degeneration. Starting at postnatal day 21, RCS rats received twice a week intraperitoneal injection of either Low Dose HNG (0.4 mg/kg), High Dose HNG (4 mg/kg), or sham-saline for 1 or 4 weeks. Visual function was tested with electroretinography (ERG) and optokinetic testing (OKT). Then the rats were euthanized for RNA, cDNA and Quantitative Real-time PCR (qRT-PCR) analysis. The results showed that high dose HNG at 4 weeks after first injection (WAFI) was associated with the largest change in gene expression in the RPE and retina of treated animals, altering expression of genes involved in apoptosis, oxidative stress, inflammation and retinal/RPE function. At 4 WAFI, ERG showed no difference between either low or high dose of HNG and sham injection, while the visual acuity tested by OKT in rats treated with high dose HNG showed significant improvement. Our findings suggested that HNG can modulate gene expression and improve vision. Further studies are warranted to show whether HNG may be a potential treatment for retinal degeneration diseases.

Keywords RCS rat model, Humanin-G, Mitochondria derived peptide, Retinal degeneration, Neuroprotection, Optokinetic testing

Mitochondrial DNA (mtDNA) (inherited maternally) can be classified into haplogroups, according to the accumulation of single nucleotide polymorphisms (SNPs). Mitochondria, with their small, but significant mtDNA, play important roles in human diseases, even when the disease is not caused directly by mitochondrial mutations[1,2]. mtDNA variants can exert major influences on cellular energy pathways as well as mediate expression of nuclear genes related to complement, inflammation, apoptosis, autophagy, methylation and cell signaling transduction pathways[3–10].

Mitochondrial Derived Peptides (MDPs) are biologically active, short peptides (20–27 AAs), which are encoded from short open reading frames (sORF) in the human mtDNA[11,12]. Humanin (HN), a 24-amino acid MDP, has been shown in vitro and in vivo to have anti-apoptotic, neuro-protective properties supporting cell survival[12–14]. Circulating HN levels decrease with age and are associated with age-related diseases in mice, rats and humans[15,16]. Furthermore, several studies showed that offspring of centenarians (people reaching the age of over 100 years) have higher HN levels compared to the general aging population[15–18]. Altogether, these findings suggest that retaining HN levels with age may promote healthy aging. HN has been shown to be cyto-protective in Alzheimer's disease, atherosclerosis, myocardial and cerebral ischemia, and Type 2 diabetes[14,19,20]. HN and SHLP2 (Small Humanin-Like Peptide 2) can lower plasma amino acids and lipid metabolites associated with metabolic aging disorders[21].

In vitro studies have shown protective effects of HN against hypoxia-induced toxicity in RGC-5 cells[22]. Pre- or co-treatment with HN protected SH-SY5Y neuroblastoma cells from toxicity induced by silver nanoparticles (AgNPs)[23]. The HNG peptide, the HN analogue, improved mitochondrial function and decreased cell death in

[1]Department of Physical Medicine and Rehabilitation, Sue and Bill Gross Stem Cell Research Center, University of California, Irvine 845 Health Sciences Road, 2035 Gross Hall, Irvine, CA 92697-1705, USA. [2]Department of Ophthalmology and Visual Science, Gavin Herbert Eye Institute, University of California Irvine, Irvine, CA 92697, USA. [3]Department of Anatomy and Neurobiology, University of California, Irvine, CA 92697, USA. [4]Bin Lin and Kevin Schneider have contributed equally to this work. ✉email: mseiler@uci.edu

PC12 cells stressed with amyloidβ25–35 peptides[24]. In human ARPE-19 retinal cybrids, HNG reduced amyloid-β induced cell stress[25]. HNG has a glycine replacing serine at position 14, making it 1000-fold more potent in its protective functions.

An in vitro animal study showed rescue of cortical neuron viability after NMDA damage following 10 µmol/L HN treatment[26]. In vivo, HN-treated diabetic mice demonstrated improved glucose tolerance and lower pancreatic-beta cell apoptosis due to activation of the Stat3 pathway[20]. HNG treatment improved the cognitive functions in aging C57B1/6 N mice and reduced the levels of inflammatory markers[27]. While studies have shown HN or HNG improve retinal cells in vitro[13,28,29], there are no studies showing their in vivo effects in retinal degeneration models.

The Royal College of Surgeons (RCS) rat is an established model for retinal degeneration. This model has dysfunctional RPE due to a MerTK mutation leading to the accumulation of outer segment debris and photoreceptor death[30], is associated with ER stress[31], and activation of mitochondrial and cytosolic calpain[32]. The RCS model has been frequently used in the preclinical testing of drugs and stem cells for retinal degeneration[33–35]. Recent studies have identified early mitochondrial dysfunction in RCS rats[36] and mtDNA deletions in the late stages of RCS retinal degeneration (> 200d)[37].

The present study investigates the effects of Humanin-G (HNG) intraperitoneal (IP) injections on the Royal College of Surgeons rat. We used twice weekly intraperitoneal injections to deliver either low dose (0.4 mg/kg) or high dose (4 mg/kg) HNG to RCS rats (starting at 21 days of age) and assessed the molecular changes in RPE cells and neuroretina, as well as vision changes at 1 week after first injection (1 WAFI) and 4 weeks after first injection (4 WAFI).

Materials and methods

HNG peptide preparation

The custom synthesized HNG peptide with guaranteed TFA removal services was purchased from Genscript Inc. (Piscataway, NJ) and diluted with sterile 0.9% saline before the injection. PLGA (Poly(lactic-co-glycolic acid)) and PVA (Polyvinyl alcohol) polymers were purchased from Akina Inc (West Lafayette, IN). Methylene Chloride was purchased from Sigma-Aldrich (St. Louis, MO). Acetonitrile, HPLC water, LC-MS water, and formic acid were purchased from Fisher Scientific (Waltham, MA). Analytical grade solvents were used in all experiments.

HNG treatments for RCS rats with retinal degeneration

Experimental animals: For all experimental procedures, animals were treated in accordance with the NIH guidelines for the care and use of laboratory animals, the ARVO Statement for the Use of Animals in Ophthalmic and Vision Research, and under a protocol approved by the Institutional Animal Care and Use Committee (AUP-17-097 and AUP 20–055). Breeding pairs of pigmented dystrophic RCS rats (RCS-p+) were obtained from Dr. Mat LaVail (University of California, San Francisco, USA). Pigmented athymic nude rats (Hsd: RH-Foxn1^{mu}, mutation in the foxn1 gene; no T cells) were purchased from Harlan Laboratories, NJ, USA. Rats were bred at University of California, Irvine (UCI) University Laboratory Animal Resources (ULAR) facilities by the Seiler laboratory. Since nude females do not lactate, non-nude females (*foxn1*+/-) were bred with nude males (*foxn1*-/-). Thus, each litter contained 50% nude and 50% non-nude rats. Sixty-three non-nude rats (*foxn1*+/-) of the immunodeficient Royal College of Surgeons (RCS) rat strain with the MERTK mutation (dysfunctional RPE) were used for the experiments[35].

Intraperitoneal injection of HNG

Starting at postnatal day 21 (P21), rats were given an intraperitoneal injection of either "Low Dose" (0.4 mg/kg) HNG; "High Dose" (4 mg/kg) HNG; or sham-saline. Injections using either 22–27 g needles were repeated twice weekly. The experiments were concluded after either 1 WAFI (short-term study) or 4 WAFI (long-term study) after the ERG and OKT tests were completed. Animals were weighed prior to each injection (HNG or saline), before the ERG and at the end of the study. The rats were monitored for any side effect (such as abnormal behavior or health issues) at routine weekly check and before any ERG and OKT tests. Any side effects were recorded.

Full field scotopic & photopic electroretinography (ERG)

For low dose HNG injection, the rats were tested with ERG, using a Rodent ERG system (Diagnosys Celeris), at 4 WAFI. For high dose injection, the rats were evaluated for changes in visual function at 1 WAFI and 4 WAFI. After overnight dark-adaptation, rats were anesthetized by intraperitoneal injection of Ketamine/Xylazine (40–55 mg/kg Ket, 6–7.5 mg/kg Xyl), then the eyes were treated with 0.5% tetracaine (Bausch & Lomb) and 1% atropine eye drops (Akorn Pharmaceuticals, Lake Forest, IL) and then anesthesia was maintained by 1% isoflurane. The rats were placed onto a heating pad on a rodent exam table and positioned in front of a monocular mini-ganzfeld photostimulator. After applying GenTeal Lubricant Eye Gel (Alcon), electrodes were placed onto the corneal surface. Visual responses with scotopic and photopic stimuli were recorded for both eyes, to obtain simultaneous recordings of the same animal using established protocols.

Optokinetic testing (OKT)

For low dose injection, the rats were tested with OKT at 4 WAFI. For high dose injection, 1 and 4 weeks after the first injection of HNG or saline, the visual acuity of RCS nude rats was measured by recording videos of optomotor responses to a virtual cylinder with alternating black and white vertical stripes (Optomotry, Cerebral Mechanics Inc., Alberta, Canada). The testing was described previously[33,38].

Rats were dark-adapted for at least 1 h prior to testing. Optomotor responses were recorded at 6 different spatial frequencies for 1 min per frequency by testers blinded to the experimental condition. Both the left and

Symbol	Gene name	Gene RefSeq number	Functions
Inflammation pathway			
DDIT3	DNA-damage inducible transcript 3	NM_001109986	This gene encodes a member of the CCAAT/enhancer-binding protein (C/EBP) family of transcription factors. The protein functions as a dominant-negative inhibitor by forming heterodimers with other C/EBP members and preventing their DNA binding activity. The protein is implicated in adipogenesis and erythropoiesis, is activated by endoplasmic reticulum stress, and promotes apoptosis. Fusion of this gene and FUS on chromosome 16 or EWSR1 on chromosome 22 induced by translocation generates chimeric proteins in myxoid liposarcomas or Ewing sarcoma. Multiple alternatively spliced transcript variants encoding two isoforms with different length have been identified.
IL6	interleukin 6	NM_012589	Enables cytokine activity and interleukin-6 receptor binding activity. Involved cellular response to lipid; positive regulation of cell communication; and response to peptide hormone. Located in cytoplasm and extracellular space.
IL1β	interleukin 1 beta	NM_031512	Enables cytokine activity. Involved in positive regulation of intracellular signal transduction; regulation of gene expression; and regulation of neurogenesis. Located in extracellular space.
TNT	tumor necrosis factor	NM_012675	Enables tumor necrosis factor receptor binding activity. Involved in positive regulation of cell communication; positive regulation of macromolecule metabolic process; and positive regulation of neuron death. Located in several cellular components, including external side of plasma membrane; extracellular space; and neuronal cell body.
HSPA5	heat shock protein family A (Hsp70) member 5	NM_013083	Enables misfolded protein binding activity and unfolded protein binding activity. Involved in cellular response to cAMP; cellular response to gamma radiation; and cellular response to metal ion. Acts upstream of or within response to endoplasmic reticulum stress. Located in membrane; mitochondrion; and smooth endoplasmic reticulum.
CCL2	C-C motif chemokine ligand 2	NM_031530	Enables chemokine activity and heparin binding activity. Involved in cellular response to cytokine stimulus; cellular response to lipid; and leukocyte migration. Located in several cellular components, including perikaryon; perinuclear region of cytoplasm; and rough endoplasmic reticulum. Colocalizes with C-fiber.
Cell cycle / hypoxia and growth factor response			
E2F1	E2F transcription factor 1	NM_001100778	Enables protein kinase binding activity and sequence-specific DNA binding activity. Involved in cellular response to hypoxia; cellular response to nerve growth factor stimulus; and positive regulation of glial cell proliferation. Located in cytoplasm and nucleus.
Antioxidant pathway			
SOD2	superoxide dismutase 2	NM_017051	Enables several functions, including identical protein binding activity; manganese ion binding activity; and superoxide dismutase activity. Involved in hydrogen peroxide biosynthetic process; negative regulation of membrane hyperpolarization; and positive regulation of hydrogen peroxide biosynthetic process. Located in mitochondrial nucleoid.
Apoptosis pathway			
BAX	bcl2 associated x	NM_017059	Enables BH domain binding activity; chaperone binding activity; and heat shock protein binding activity. Involved in glial cell apoptotic process; mitochondrion organization; and response to corticosterone. Located in cytosol; mitochondrial outer membrane; and perinuclear region of cytoplasm.
BCL2L1	bcl2-like 1	NM_001033672	Enables several functions, including GTPase binding activity; MDM2/MDM4 family protein binding activity; and cysteine-type endopeptidase inhibitor activity involved in apoptotic process. Involved in cellular response to cytokine stimulus; cellular response to lipid; and positive regulation of transport. Located in cytosol; mitochondrial outer membrane; and presynapse. Colocalizes with clathrin-coated pit; mitochondrial membrane; and synaptic vesicle membrane.
BCL2L13	bcl2-like 13	NM_001398849	Over-expression leads to apoptosis. Mitochondria specific protein.
CASP3	caspase 3	NM_012922	Enables death receptor binding activity; phospholipase A2 activator activity; and protease binding activity. Involved in luteolysis; nervous system development; and positive regulation of amyloid-beta formation. Located in cytosol; membrane raft; and neuronal cell body. Part of death-inducing signaling complex.
CASP7	caspase 7	NM_022260	Enables cysteine-type peptidase activity. Involved in aging; leukocyte apoptotic process; and striated muscle cell differentiation. Located in cytosol and intracellular membrane-bounded organelle.
CASP9	caspase 9	NM_031632	Enables cysteine-type peptidase activity. Involved in glial cell apoptotic process; response to estradiol; and response to ischemia. Located in cytosol; mitochondrion; and nucleus.
Photoreceptor markers			
CRX	cone-rod homeobox	NM_021855	Enables DNA binding activity. Involved in circadian rhythm and positive regulation of photoreceptor cell differentiation. Located in nucleus.
ROM1	retinal outer segment membrane protein 1	NM_001009690	Predicted to enable protein homodimerization activity; be involved in cell adhesion; act upstream of or within detection of light stimulus involved in visual perception; protein complex oligomerization; and retina development in camera-type eye. Predicted to be located in photoreceptor outer segment membrane and an integral component of plasma membrane.
NRL	neural retina leucine zipper	NM_001106036	Predicted to enable DNA-binding transcription activator activity, RNA polymerase II-specific; leucine zipper domain binding activity; and promoter-specific chromatin binding activity. Predicted to be involved in regulation of transcription by RNA polymerase II and retinal rod cell development and to act upstream of or within positive regulation of gene expression and positive regulation of transcription by RNA polymerase II. Predicted to be located in cytosol and nucleoplasm and to be active in nucleus.
GNGT1	G protein subunit gamma transducin 1	NM_001135777	Predicted to enable G-protein beta-subunit binding activity. Acts upstream of or within cardiac muscle cell apoptotic process and cellular response to hypoxia. Located in photoreceptor inner segment and photoreceptor outer segment. Part of heterotrimeric G-protein complex.
RPE markers			
RLBP1	Encodes cellular retinaldehyde binding protein (CRALBP)	NM_000326	Expressed both in RPE and in retinal Müller glia. *RLBP1* encodes retinaldehyde-binding protein 1, a water-soluble lipid-binding protein that carries 11-cis-retinaldehyde and 11-cis-retinal as physiologic ligands. It is a functional component of the visual cycle and is involved in vitamin A metabolic process and visual perception. *RLBP1* supports transport steps in visual-cycle metabolism that connect vitamin A handling to light-dependent vision.
RPE65	retinoid isomerohydrolase retinal pigment epithelium-specific 65 kDa protein	NM_053562	Enables all-trans-retinyl-ester hydrolase, 11-cis retinol forming activity. Involved in circadian rhythm; neural retina development; and retinoid metabolic process. Located in cell body.
TJP1	tight junction protein 1	NM_001106266	Enables protein C-terminus binding activity. Involved in cellular response to glucose stimulus; negative regulation of vascular permeability; and response to lipopolysaccharide. Located in bicellular tight junction; cytoplasm; and gap junction.
Continued			

Symbol	Gene name	Gene RefSeq number	Functions
BEST1	Bestrophin 1	NM_001011940	Predicted to enable identical protein binding activity; to contribute to chloride channel activity; to be involved in transepithelial chloride transport; to act upstream of or within chloride transport; detection of light stimulus involved in visual perception; and regulation of calcium ion transport. Predicted to be located in basolateral plasma membrane. Predicted to be part of chloride channel complex.
Housekeeper			
HMBS	hydroxymethylbilane synthase	NM_013168	Part of the hydroxymethylbilane synthase superfamily in which the gene product is the third enzyme in the heme biosynthetic pathway and serves as a catalyst for the head to tail condensation of four molecules of porphobilinogen into the linear hydroxymethylbilane.

Table 1. Description of genes analyzed by qRT-PCR.

right eyes were tested by alternating the direction of the moving stripes. Two independent tests were performed at each time point, with at least one hour in between; one test going from lowest to highest frequency, and the other from highest to lowest frequency. The best visual acuity of the two tests was used for analysis. All tests were video recorded and evaluated off-line by two independent observers blinded to the experimental conditions. Any discrepancies between the two observers resulted in re-analysis of videos by a third observer, and data discussion before giving a final score, and prior to decoding the experimental condition.

Isolation of tissue, RNA and amplification of cDNA

Rats were euthanized by CO_2 asphyxiation using IACUC-approved methods. Rats were exposed to CO_2 for 10 min., followed by cervical dislocation. Then eyes were enucleated. Upon removal of the anterior segment of the eye including the cornea, iris and lens, the retina was removed and immediately snap frozen in liquid nitrogen. The RPE was isolated by utilizing the "Simultaneous RPE cell Isolation and RNA Stabilization" (SRIRS method)[39]. The posterior eye cup including the choroid, sclera and RPE was removed and immediately placed in a microcentrifuge tube containing 400 µl of RNAprotect cell reagent (Qiagen). After a minimum of 10 min, the tube was agitated and RPE cells observed to be released into solution. The eye cup was then removed and the dissociated RPE cells pelleted. This provided selective isolation of the RPE and protection against RNA degradation in one step. RNA was isolated from RPE cells and the neuroretina using the PureLink RNA mini kit. cDNA was produced using SuperScript IV VILO (ThermoFisher) according to the manufacturer's instructions.

Quantitative real-time PCR (qRT-PCR) analyses

qRT-PCR was performed on individual samples using PowerUp SYBR Green Master Mix (ThermoFisher Scientific) on an Applied Biosystems QuantStudio 5 Real-Time PCR system real time quantitative PCR detection system. Primers (QuantiTect Primer Assay (Qiagen) or KiCqStart Primers (Sigma)) were used to analyze 24 different genes: Inflammation and oxidative stress (*DDIT3*, *HSPα5*, *IL6*, *IL1β*, *TNFα*, *CCL2*); Cell cycle, hypoxia and growth factor response (*E2F1*), Apoptosis (*BAX*, *CASP3*, *CASP7*, *CASP9*, *BCL2L1*, *BCL2L13*); Antioxidation (*SOD2*); Photoreceptor markers (*CRX*, *GNGT1*, *NRL*, *ROM1*); and RPE markers (*BEST1*, *RLBP1*, *RPE65*, *TJP1*) (Table 1). Primers were standardized with the HMBS housekeeping gene. All analyses were performed in triplicate. The fold values were calculated using the 2^(-ΔΔCt) formula. All fold value changes of the HNG-IP treatments were calculated compared with saline control.

Statistical analysis

Statistical analysis was performed using Graphpad Prism, using t-tests (paired or unpaired Mann-Whitney U test). The significance level was set at $p < 0.05$.

Results

Intraperitoneal HNG injection studies

Animals were weighed and monitored for any side effect (such as abnormal behavior or health issues) routinely. No side effects were observed throughout the study. No change in behavior was found. We found no significant changes in the weights between the saline and HNG groups at any testing condition, whether it was short term, long term, high dose (saline group: $n = 9$. HNG group: $n = 11$) or low dose (saline group: $n = 4$. HNG group: $n = 4$). Figure 1 showed the example of weights compared to baseline at the longest treatment time, with the highest dose: high dose group (saline group: $n = 9$; HNG group: $n = 11$) at the end of the study (4 WAFI). There were no significant differences in male and female rats between the HNG group and the saline group.

Retinal gene expression levels after intraperitoneal HNG injection

Gene expression for IP low dose HNG (0.4 mg/kg) at 1 WAFI

The RPE showed a significant increase in expression of the inflammation marker *TNFα* (1.789-fold, $P = 0.0023$) and a significant decrease in expression of *RLBP1* (cellular retinal binding protein) (0.6781-fold, $P = 0.0271$) in animals treated with low dose HNG for 1 week ($n = 4$) compared to saline group ($n = 4$) (Supplemental Table 1). There were no statistically significant changes in gene expression in the neuroretina of animals treated with low dose HNG for 1 week ($n = 4$) compared to saline group ($n = 4$).

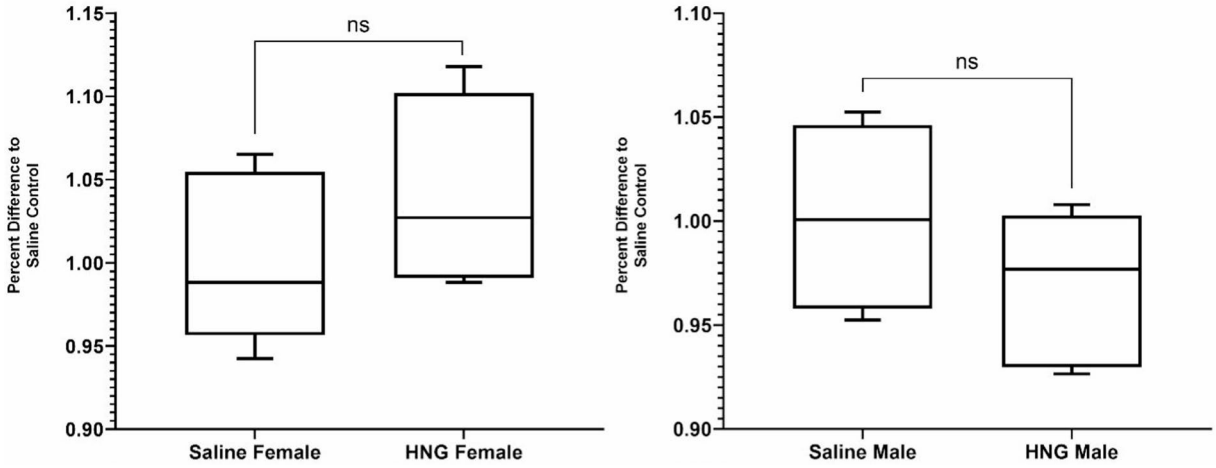


Fig. 1. No change in animal weight between the HNG high dose and the saline groups at 4 WAFI. All weight data were normalized to the weight before HNG or saline injection (Mean ± SEM). Example of the longest treatment time, with the highest dose: High dose group (saline group: $n = 9$. HNG group: $n = 11$) at the end of the study (4 WAFI). No significant differences in the male and female rats between the HNG group and the saline group. ns: no significant.

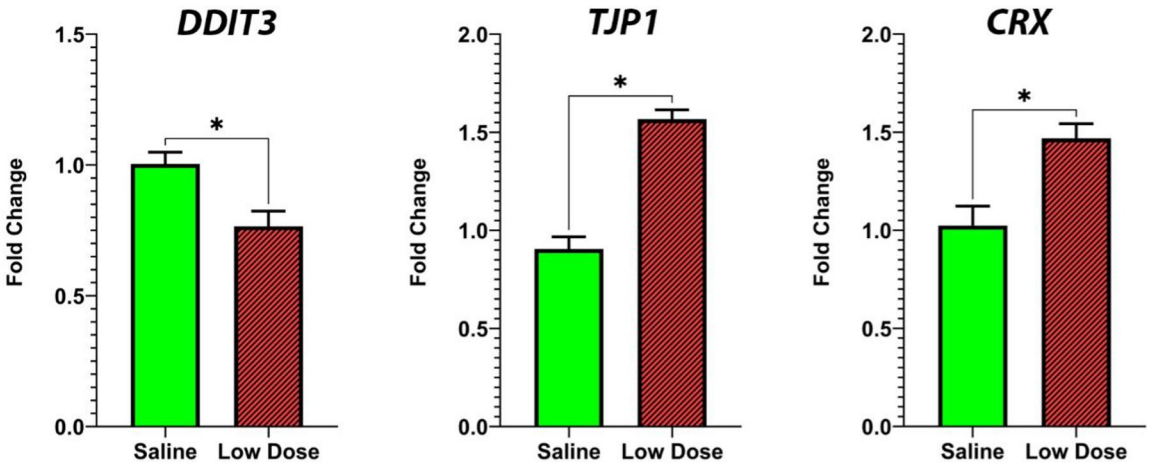


Fig. 2. Effect of Low dose (0.4 mg/kg) HNG on gene expression in neuroretina at 4 WAFI. Expression of *DDIT3* was significantly decreased and expression of *TJP1* and *CRX* were significantly increased at 4 WAFI with low dose HNG ($n = 5$) compared with saline ($n = 4$) in the neuroretina. Mean ± SEM. *: $p < 0.05$. See also Supplemental Table 2.

Gene expression for IP low dose HNG (0.4 mg/kg) at 4 WAFI

The neuroretina showed decreased levels of proapoptotic *DDIT3* (0.7658-fold, $P = 0.0159$) and increased levels of the photoreceptor marker CRX (1.468-fold, $P = 0.0357$) and tight junction marker *TJP1* (1.567-fold, $P = 0.0286$) in the low dose HNG group ($n = 5$) compared to the saline group ($n = 4$) at 4 WAFI (Fig. 2; Supplemental Table 2). The RPE cells demonstrated no significant changes in gene expression.

Gene expression for IP high dose HNG (4 mg/kg) at 1 WAFI

In the RCS rats treated with High Dose HNG ($n = 9$), the RPE showed decreased expression levels of the apoptotic genes (*BCL2L1*, 0.587-fold, $P = 0.0190$) and *CASP7* (0.5737-fold, $P = 0.0321$) compared to the saline treated samples ($n = 9$) (Fig. 3a, Supplemental Table 3). The neuroretina showed increased levels of *CRX* (1.309-fold, $P = 0.0103$) in HNG group (Fig. 3b). There were no statistically significant changes in other genes' expression.

Gene expression for IP high dose HNG (4 mg/kg) at 4 WAFI

The RPE showed increased expression levels of pro-apoptotic genes (*DDIT3*, 1.842-fold, $P = 0.0317$; *CASP3*,1.65-fold, $P = 0.0079$); inflammation genes (*IL6*, 1.782-fold, $P = 0.0286$); antioxidant genes (SOD2, 1.797-fold, 0.0286); and RPE genes important for normal function (*BEST1*, 1.698-fold, $P = 0.0317$) in the HNG group ($n = 11$) vs. the saline group ($n = 9$) (Fig. 4a, Supplemental Table 4). There was also a lower expression level of the cell cycle

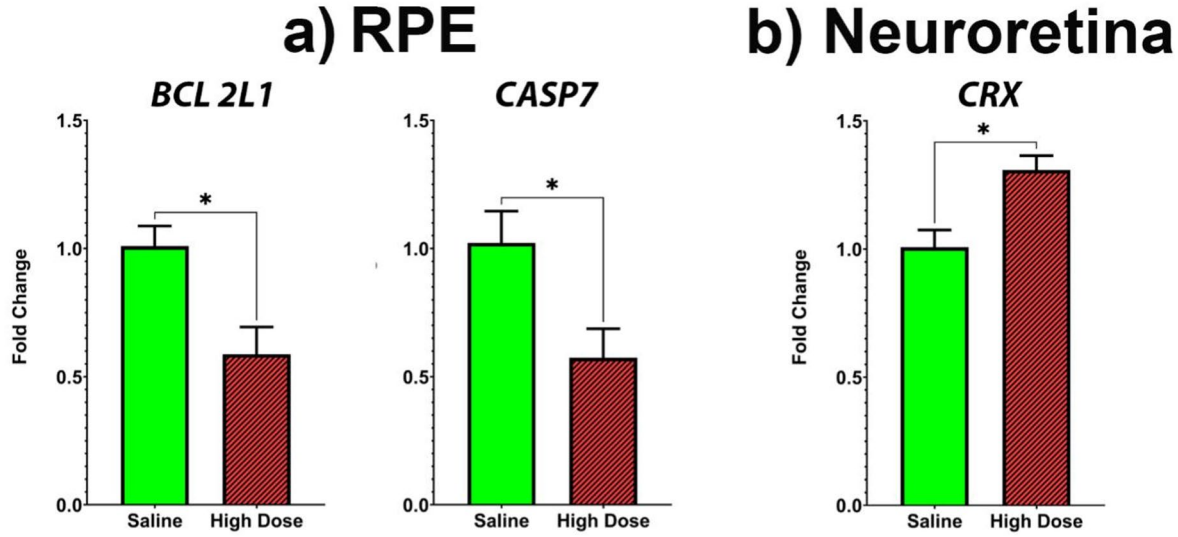


Fig. 3. Effect of High dose (4.0 mg/kg) HNG on gene expression in the RPE and Neuroretina at 1 WAFI. (**a**) Expression of *BCL2L1* and *CASP7* was significantly decreased at 1 WAFI with high dose HNG ($n = 9$) compared with saline ($n = 9$) in the RPE. (**b**) Expression of *CRX* was significantly increased at 1 WAFI with high dose HNG ($n = 9$) compared with saline ($n = 9$) in the neuroretina. Mean ± SEM. *: $p < 0.05$. See also Supplemental Table 3.

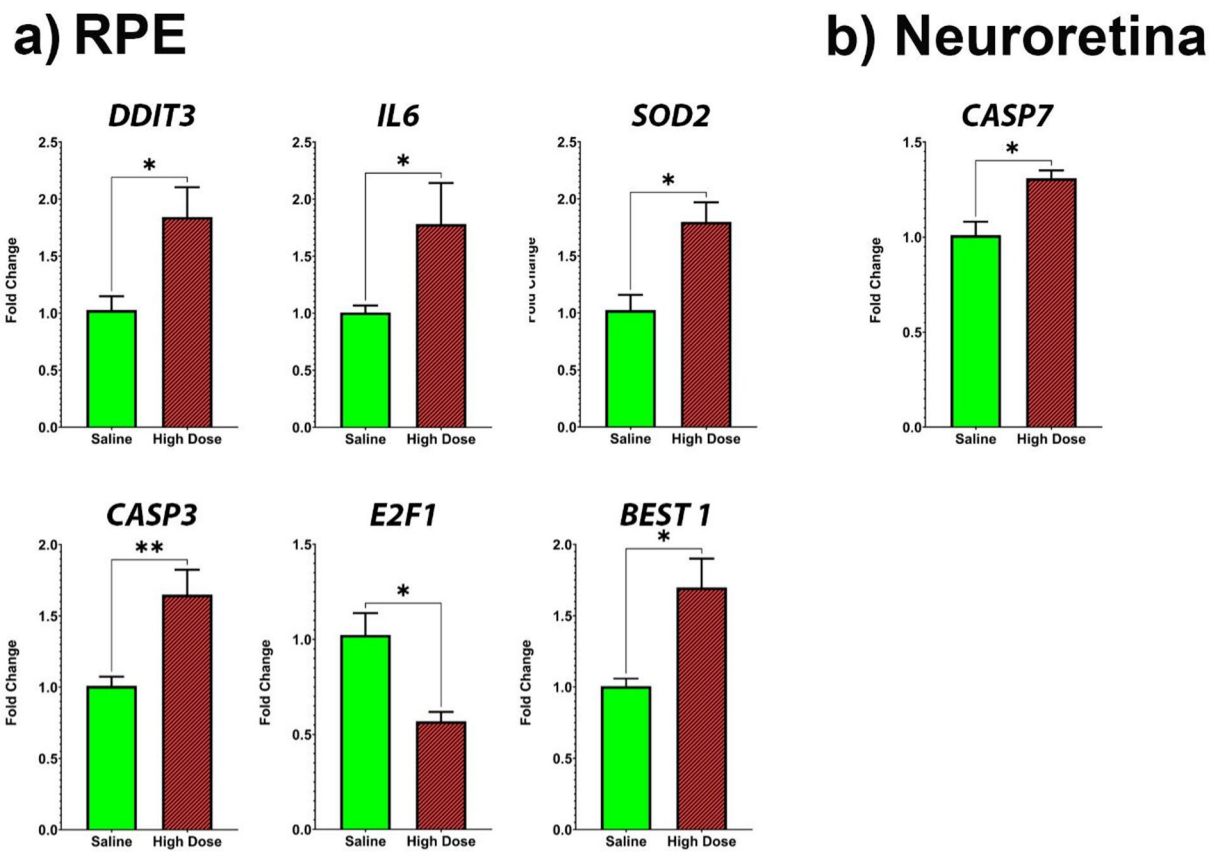


Fig. 4. Effect of High dose (4.0 mg/kg) HNG on gene expression in the RPE and Neuroretina at 4 WAFI. (**a**) In the RPE, expression of *DDIT3*, *IL6*, *SOD2*, *CASP3*, and *BEST1* were all significantly increased, and *E2F1* was significantly decreased at 4 WAFI with high dose HNG ($n = 11$) compared with saline ($n = 9$). (**b**) In the neuroretina, expression of *CASP7* was significantly increased at 4 WAFI with high dose HNG ($n = 11$) compared with saline ($n = 9$). Mean ± SEM. *: $p < 0.05$. **: $p < 0.01$. See also Supplemental Table 4.

transcription factor *E2F1* (which is activated in response to hypoxia and growth factors) (0.569-fold, $P=0.016$) in the RPE of the HNG group. The neuroretina of the HNG group showed increased levels of proapoptotic *CASP7* (1.309-fold, $P=0.0159$) (Fig. 4b; Table 4). There were no statistically significant changes in the expression of other genes.

Results of ERG at 1 and 4 WAFI

The ERG analyses were performed first on Low Dose HNG (0.4 mg/kg), and Sham-Saline at 4 WAFI. There was no difference between Low Dose HNG ($n=5$) and Saline ($n=5$) in a-wave and b-wave of scotopic and photopic full field ERG (Fig. 5e and f). Later, High Dose HNG (4 mg/kg) and Saline groups were tested with ERG. At 1 and 4 WAFI, there was no significant difference in scotopic and photopic a-wave (data not shown), or scotopic

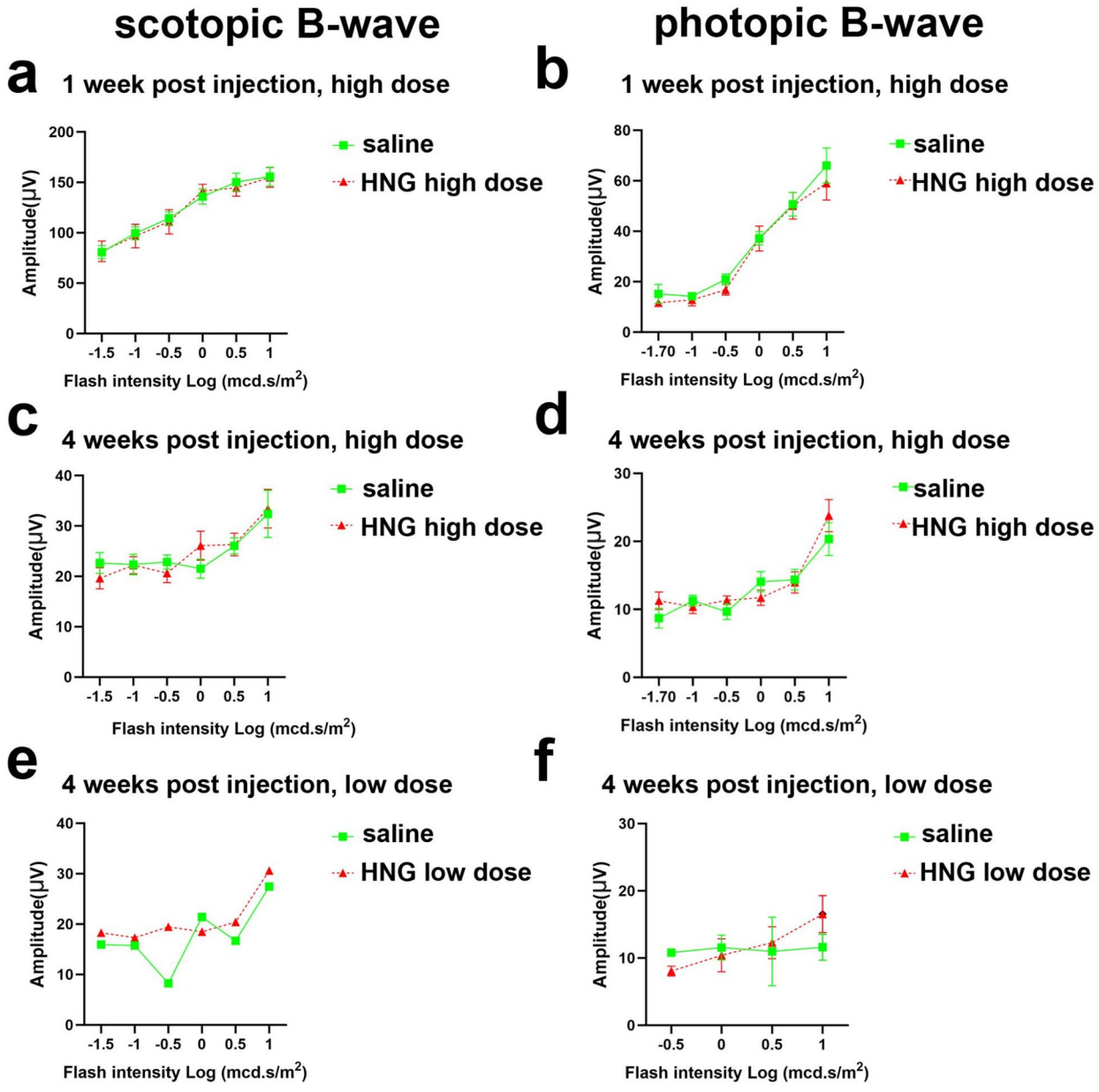


Fig. 5. ERG Results from low (0.4 mg/kg) and high dose (4 mg/kg) IP Injections at 1 and 4 WAFI. (**a**) Scotopic B-wave showed no difference between high dose HNG ($n=13$) from the saline group ($n=9$) at 1 WAFI. (**b**) Photopic B-wave showed no difference between high dose HNG ($n=13$) from the saline group ($n=9$) at 1 WAFI. (**c**) Scotopic B-wave showed no difference between high dose HNG ($n=12$) from the saline group ($n=9$) at 4 WAFI. (**d**) Photopic B-wave showed no difference between high dose HNG ($n=12$) from the saline group ($n=9$) at 4 WAFI. (**e**) Scotopic B-wave showed no difference between low dose HNG ($n=5$) from the saline group ($n=5$) at 4 WAFI. (**f**) Photopic B-wave showed no difference between low dose HNG ($n=5$) from the saline group ($n=5$) at 4 WAFI. Mean ± SEM. See also Supplemental Table 5.

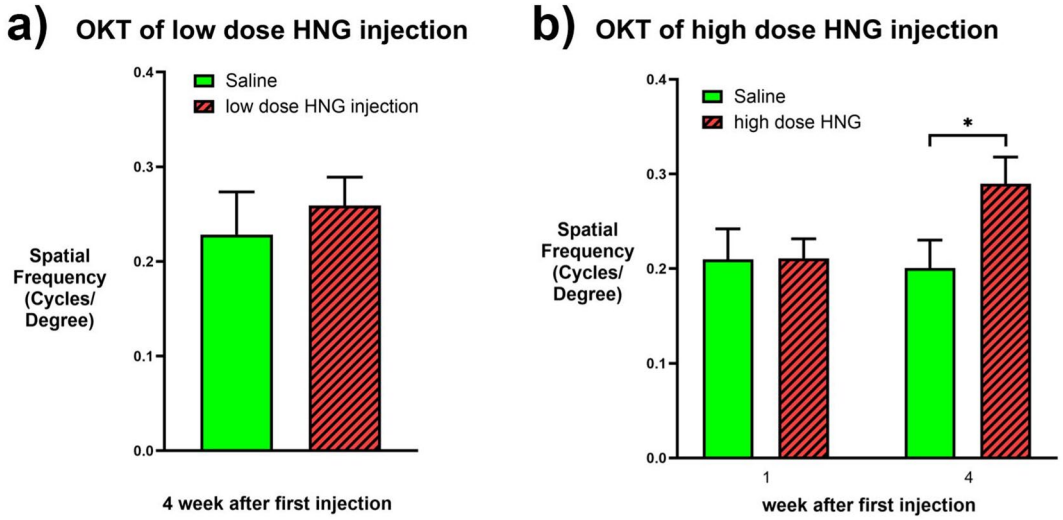


Fig. 6. Effect of high dose IP injections of HNG on OKT at both 1 WAFI and 4 WAFI. (**a**) At 4 WAFI, optokinetic testing in RCS rats showed that the visual acuity of the eyes in the low dose HNG group ($n = 4$) is better than that of the saline group ($n = 4$) but the difference is not significant. (**b**) At 1 WAFI, there is no difference between the high dose group ($n = 11$) and the saline group ($n = 10$); however, at 4 WAFI, the high dose HNG ($n = 11$) showed significant improvement from that of saline groups ($n = 9$. $p < 0.05$). Mean ± SEM. *: $p < 0.05$. See also Supplemental Table 6.

and photopic b-wave between High dose HNG (1 WAFI: $n = 13$. 4 WAFI: $n = 12$) and Sham-Saline groups ($n = 9$) (Fig. 5a–d; Supplemental Table 5).

Visual function improvement evaluated by optokinetic testing (OKT)

At 4 WAFI, optokinetic testing in RCS rats showed that the visual acuity of eyes with the low dose HNG group ($n = 4$) was better than the saline group ($n = 4$) but the difference was not significant (Fig. 6a). At 1 WAFI, there was no difference between the high dose group ($n = 11$) and the saline group ($n = 10$); however, at 4 WAFI, the high dose HNG group ($n = 11$) showed significant improvement from that of saline groups ($n = 9$. $p < 0.05$) (Fig. 6b) (data in Supplemental Table 6).

Discussion

HNG has demonstrated cytoprotective effects in human cybrid cell lines and animal models of neurodegeneration[40,41]. In a study evaluating an analog of Humanin in ameliorating streptozotocin-induced diabetic nephropathy in Sprague Dawley rats, [S14G]-humanin was administered intra-peritoneal (once daily for a course of 16 weeks) at a dosage of 0.4 mg/kg of body weight[42]. Another study reported that humanin exhibits neuroprotective effects in vitro in human cell culture models and enhances cognition in vivo in aged mice[27]. In the present study, we used twice weekly intraperitoneal injections to deliver either low dose (0.4 mg/kg) or high dose (4 mg/kg) HNG to RCS rats and showed that HNG IP injections can modulate in RPE and neuroretina gene expression levels and in the short-term, improve optokinetic visual function in the RCS rat model.

The low dose IP injections at 1 WAFI resulted in upregulation of the inflammation marker *TNFα* and downregulation of *RLBP1*, the gene for cellular retinal binding protein, in the RPE cells, whereas by 4 WAFI, no significant changes in gene expression were observed across all pathways. In a rat model of ulcerative colitis, intraperitoneal HNG (10 or 20 µM) reduced expression of inflammatory markers *TNFα* and *Il-1β* and decreased the apoptotic marker Caspase 3 activities[43]. Similarly, in a rat model of pituitary tumors, 5 µM HN inhibited the proapoptotic effect of *TNFα* on cultured anterior pituitary cells[44]. In ApoE deficient mice on a high-cholesterol diet, after 16 weeks of intraperitoneal HN (4 mg/kg/day) treatment, the inflammatory markers *TNFα*, MCP-1 and osteopontin were downregulated, along with decreased apoptosis, compared to the untreated ApoE-/- mice[45]. Similar decline in the pro-inflammatory *TNFα* and *IL-1β* were seen after HN treatment in HUVEC culture[19].

TNFα is a key pivotal mediator of inflammation in AMD, known for disrupting endothelial integrity and initiating inflammatory pathways that accelerate disease progression[46,47]. However, studies assessing TNFα level in aqueous humour or in serum remain inconclusive[48–50]. Although TNFα is theoretically expected to be elevated in AMD, most comparisons between AMD and control groups have shown no significant differences[49,50]. Furthermore, TNFα was significantly higher in patients who improved than in those who deteriorated[49].

Overall, systemic and local measurements of TNFα remain inconsistent. While TNFα inhibition is effective for some ocular diseases such as uveitis[51], clinical outcomes for anti-TNFα therapy in AMD, whether systemic[52] or intravitreal[53], have been variable. Future studies should clarify these discrepancies.

Our observation of elevated TNFα at 1 WAFI may reflect either the uncertain role of TNFα or the short duration and low dose of treatment, particularly since no change was observed at 4 WAFI. Further investigation is warranted.

RLBP1 encodes cellular retinal-binding protein (CRALBP), an 11-cis-retinal–binding protein expressed in Müller and RPE cells[54], and is essential for the visual cycle. RLBP1 mutations cause three clinical subtypes—Bothnia dystrophy, retinitis punctata albescens, and Newfoundland rod-cone dystrophy[55]. Gene therapy using AAV vectors expressing RLBP1 has improved the visual cycle in RLBP1−/− mice[56] and in patients with RLBP1-associated retinal dystrophy[57]. We observed downregulation of RLBP1 in RPE cells at 1 WAFI but not at 4 WAFI. Further studies are needed.

Interestingly, at 1 WAFI, no gene expression changes were seen for any of the neuroretinal genes, suggesting that either higher HNG doses or a longer exposure is required to modulate the neuroretinal genes. By 4 WAFI, *DDIT3* was significantly downregulated ($p = 0.0159$), while *TJP1* ($p = 0.0286$) and *CRX* ($p = 0.0357$) were upregulated. The DNA damage inducible transcript 3 *(DDIT3*, also known as transcription factor *C/EBP-homologous protein*, *CHOP)* is an ER stress effector that promotes ER stress and the subsequent inflammation and apoptosis induced by lipopolysaccharide (LPS) exposure[58,59].

DDIT3 is implicated in neurodegeneration. Human RPE cybrids harboring AMD mitochondria show markedly elevated *DDIT3* (also known as CHOP, 633.9%), Caspase-3 (125.7%), and Caspase-7 (181.3%) levels, with reduced *E2F1* (66.2%) and *SOD2* levels (23.1%) compared to the cybrids with age-matched normal mitochondria. HNG treatment significantly reduces these pro-apoptotic and ER stress markers[10,25]. In primary human RPE cell cultures, HN pretreatment decreases ER-stress induced apoptosis by elevating mitochondria glutathione and lowering CHOP (DDIT3) levels[29]. Similarly, Sreekumar et al. demonstrated that HN localizes to RPE cells and protected against oxidative stress by improving mitochondrial biogenesis and bioenergetics[13]. In our study, the expression of DDIT3 was reduced at 4 WAFI with low dose HNG (which would confirm neuroprotection), but increased with high dose HNG which is contradictory. This issue needs to be further explored.

Tight junction protein-1 (TJP1), also known as the tight junction marker ZO-1, is a peripheral membrane phosphoprotein of the zonula occludens family and a key component linking junctional proteins to the cytoskeleton to maintain epithelial integrity[60]. Reduced ZO-1 expression in RPE cells is associated with epithelial–mesenchymal transition and compromised retinal support[60,61], leading to pathologies such as age-related macular degeneration (AMD) and diabetic retinopathy[60,61]. Thus, our data, HNG-induced upregulation of TJP1, suggests its potential to preserve RPE integrity and treat AMD.

CRX (cone–rod homeobox) is a transcription factor critical for photoreceptor development and differentiation, regulating numerous phototransduction and metabolic genes[62]. Dysregulated CRX–Otx2 interaction contributes to early-onset retinal degeneration[63]. Mutations in upstream regulators of CRX–Otx2 disrupt gene activation balance, causing aberrant photoreceptor gene expression and apoptosis[63]. CRX also partners with NRL and Nr2e3 to promote rod-specific gene expression while suppressing cone genes during differentiation[62]. Loss or mutation of CRX results in photoreceptor degeneration and disorders such as Leber congenital amaurosis (LCA) and cone–rod dystrophy[64]. In our study, HNG-induced upregulation of CRX further supports its potential as a therapeutic agent for AMD.

As expected, high-dose HNG altered the expression of more genes than low-dose HNG. At 1 WAFI, HNG-treated RPE cells showed downregulation of the pro-apoptotic gene CASP7 ($p = 0.0321$) and the anti-apoptotic BCL2L1 ($p = 0.0189$). While the latter appears inconsistent with HNG's beneficial effects, BCL2L1 has multiple cellular roles. BCL2L1 encodes the anti-apoptotic protein BCL-XL[65], which provides a strong selective advantage to human pluripotent stem cells (hPSCs) under stress conditions such as thawing, expansion, and cloning[65]. BCL-XL localizes mitochondria to prevent cytochrome C release and Caspase-dependent apoptosis through interactions with other BCL-2 family members[66]. Beyond its anti-apoptotic role, BCL-XL contributes to metabolism, mitochondrial dynamics, and calcium homeostasis[66], and has been implicated in regulating cell fate by inhibiting neuroectodermal differentiation[67]. In RPE tissue and ARPE19 cells, BCL-XL supports cell survival[68], but persistent expression in senescent RPE cells contributes to apoptosis resistance and tissue dysfunction in aging and AMD models[67,69,70]. Inhibiting BCL-XL in senescent RPE is therefore a promising therapeutic approach for AMD[69,70]. Given its roles in mitochondrial and calcium homeostasis—critical to RPE physiology—the downregulation of BCL2L1 by HNG may also contribute to its protective effects.

At 4 WAFI, high-dose HNG altered more genes (6 vs. 0) than the low dose in RPE cells, including upregulation of pro-apoptotic (CASP3), ER stress (DDIT3), inflammatory (Il-6), antioxidant (SOD2), and RPE marker (BEST1) genes, while E2F1 expression was significantly reduced. E2F1 is a transcription factor regulating genes involved in DNA replication, repair, the cell cycle, and apoptosis[71]. Its biological functions are modulated by post-translational modifications[72]. IL-6 is a pleiotropic cytokine that primarily acts as a pro-inflammatory factor[73]. In RPE cells, IL-6 inhibits Sirt1 through PI3K/AKT/mTOR-mediated phosphorylation, suppressing the E2F1/HMGA1/G6PD pathway and thereby increasing oxidative stress and cell death[74]. Although HNG increased CASP3, DDIT3, and Il-6 while reducing E2F1, these changes may reflect alternative functions and warrant further investigation.

Superoxide dismutases (SODs) are critical antioxidant enzymes that prevent oxidative stress by metabolizing reactive oxygen species (ROS)[75]. SOD2, localized in mitochondria, detoxifies superoxide radicals generated during oxidative phosphorylation at complexes I and III, converting them into hydrogen peroxide and oxygen[76]. Upregulation of SOD2 reduces oxidative stress, supporting mitochondrial protection, a key factor in neurodegenerative disease mitigation[77]. Thus, HNG-induced SOD2 upregulation suggests a potential therapeutic mechanism.

The BEST gene family encodes Ca^{2+}-activated anion channels with diverse physiological roles in multiple organs, including the eye[78]. BEST1 is predominantly expressed in RPE cells and is genetically associated with

various retinal degenerations[79], encompassing over 350 known mutations leading to progressive vision loss and blindness[80]. Given BEST1's critical function in retinal health and its link to untreatable vision disorders, the observed BEST1 upregulation by HNG further supports its therapeutic potential in retinal degenerative diseases.

At 1 WAFI, the neuroretina exhibited elevated *CRX* expression ($p = 0.0103$), while other genes remained comparable to saline-treated controls. As described above, *CRX* regulates multiple photoreceptor-specific genes essential for photoreceptor development and differentiation. Its upregulation supports the beneficial effect of HNG in retinal degeneration (RD) diseases. At 4 WAFI, *CASP7* expression increased ($p = 0.0159$), whereas other genes remained unchanged relative to controls. Overall, more genes were modulated in RPE cells (six genes) than in neuroretina (one gene), likely due to the reduced neuroretinal thickness in RCS rats by 30 days or a greater sensitivity of RPE cells to HN-mediated protection. Sreekumar et al. reported that polarized human RPE cells contain high intracellular HN co-localized with mitochondria[13]. Exogenous FITC-labeled HN peptides showed robust uptake and mitochondrial translocation in RPE cells compared to controls, indicating a mitochondria-targeted protective role. Moreover, RPE cells express all three HN receptors—ciliary neurotrophic factor receptor (CNTFRα), transmembrane glycoprotein gp130 (GP130), and cytokine receptor WSX1[13,29]—which may account for the stronger HNG effects observed in RPE cells than in neuroretina.

No significant differences were observed in scotopic or photopic a- and b-wave amplitudes between high-dose, low-dose HNG, and sham-saline groups. The absence of detectable ERG changes at 1 WAFI may reflect the single early injection and the time required for HNG to exert measurable effects. By 4 WAFI, the rapid retinal degeneration characteristic of the RCS rat resulted in undetectable ERG responses across all groups. Therefore, a potential beneficial effect of HNG cannot be excluded, as ERG may lack the sensitivity to detect subtle improvements. Interestingly, while no improvement in OKT was seen at 1 WAFI following high-dose intraperitoneal HNG, visual function improved at 4 WAFI. Molecular analyses revealed increased expression of several genes in both neuroretina and RPE tissues, suggesting that intraperitoneally administered HNG may cross the blood–retina barrier or induce systemic changes affecting these tissues.

Because intraperitoneal injections have shown effects on cognition in mice, and thus appear to pass the blood-brain barrier[17,27,41], we used the same approach in our study. However, we only performed biweekly (not daily) intraperitoneal injections, and it is unknown how much HNG reaches the retina and how fast it gets degraded. Administration of HNG in a slower degradable form (e.g. microspheres) and closer to the eye may improve its effects. A limitation of our study is that we could not measure humanin levels in the eye because it was not possible for us to distinguish between intrinsic and added humanin.

Nevertheless, intraperitoneal HNG administration in the RCS rat model modulated the expression of genes related to Inflammation and oxidative stress, cell cycle, hypoxia, growth factor response, apoptosis, antioxidation, photoreceptor and RPE function, in RPE and neuroretina. The data suggested a possible blood–retina barrier penetration or systemic regulation of HNG, consistent with other studies[17,21,27,41], and HNG as a potential treatment for retinal degeneration diseases. Although the regulation of some genes seemed to be contradictory, it may be caused by the complications of the gene functions. For example, TNFα is a key mediator of inflammation in AMD[46,47] and is theoretically expected to be elevated in AMD, but most comparisons between AMD and control groups have shown no significant differences[49,50]. Furthermore, TNFα was significantly higher in patients who improved than in those who deteriorated[49]. While TNFα inhibition is effective for some ocular diseases such as uveitis[51], clinical outcomes for anti-TNFα therapy in AMD have been variable[52,53]. Although ERG data didn't show any difference, the improved visual performance at 4 WAFI as measured by OKT did support the neuroprotective effect of HNG. It is the first in vivo study of HNG on the retinal disease. Further study will be needed to optimize the dose and the way of delivery. And of course it will be interesting to study the mechanism behind it.

Data availability

All data generated or analyzed during this study are included in this article. Further enquiries can be directed at the corresponding author.

Received: 30 April 2026; Accepted: 14 July 2026
Published online: 18 July 2026

References

1. Czarnecka, A. M. & Bartnik, E. The role of the mitochondrial genome in ageing and carcinogenesis. *J. Aging Res.* **2011**, 136435. https://doi.org/10.4061/2011/136435 (2011).
2. Wallace, D. C. & Fan, W. Energetics, epigenetics, mitochondrial genetics. *Mitochondrion* **10**, 12–31. https://doi.org/10.1016/j.mito.2009.09.006 (2010).
3. Atilano, S. R. et al. Differential epigenetic status and responses to stressors between retinal cybrids cells with African versus European mitochondrial DNA: Insights into disease susceptibilities. *Cells* **11**. https://doi.org/10.3390/cells11172655 (2022).
4. Atilano, S. R. et al. Mitochondrial DNA variants can mediate methylation status of inflammation, angiogenesis and signaling genes. *Hum. Mol. Genet.* **24**, 4491–4503. https://doi.org/10.1093/hmg/ddv173 (2015).
5. Dolinko, A. H. et al. Hypoxia-induced transcriptional differences in African and Asian versus European diabetic cybrids. *Sci. Rep.* **13**, 3818. https://doi.org/10.1038/s41598-023-30518-x (2023).
6. Kenney, M. C. et al. Inherited mitochondrial DNA variants can affect complement, inflammation and apoptosis pathways: Insights into mitochondrial-nuclear interactions. *Hum. Mol. Genet.* **23**, 3537–3551. https://doi.org/10.1093/hmg/ddu065 (2014).
7. Kenney, M. C. et al. Molecular and bioenergetic differences between cells with African versus European inherited mitochondrial DNA haplogroups: Implications for population susceptibility to diseases. *Biochim. Biophys. Acta* **1842**, 208–219. https://doi.org/10.1016/j.bbadis.2013.10.016 (2014).
8. Kenney, M. C. et al. Mitochondrial DNA variants mediate energy production and expression levels for CFH, C3 and EFEMP1 genes: Implications for age-related macular degeneration. *PLoS One* **8**, e54339. https://doi.org/10.1371/journal.pone.0054339 (2013).

9. Malik, D. et al. Human retinal transmitochondrial cybrids with J or H mtDNA haplogroups respond differently to ultraviolet radiation: Implications for retinal diseases. *PLoS One* **9**, e99003. https://doi.org/10.1371/journal.pone.0099003 (2014).
10. Nashine, S. & Kenney, M. C. Effects of Humanin G (HNG) on angiogenesis and neurodegeneration markers in Age-related Macular Degeneration (AMD). *Mitochondrion* **74**, 101818. https://doi.org/10.1016/j.mito.2023.11.001 (2024).
11. Gong, Z. & Tasset, I. Humanin enhances the cellular response to stress by activation of chaperone-mediated autophagy. *Oncotarget* **9**, 10832–10833. https://doi.org/10.18632/oncotarget.24396 (2018).
12. Lee, C. et al. IGF-I regulates the age-dependent signaling peptide humanin. *Aging Cell.* **13**, 958–961. https://doi.org/10.1111/acel.12243 (2014).
13. Sreekumar, P. G. et al. The mitochondrial-derived peptide humanin protects RPE cells from oxidative stress, senescence, and mitochondrial dysfunction. *Invest. Ophthalmol. Vis. Sci.* **57**, 1238–1253. https://doi.org/10.1167/iovs.15-17053 (2016).
14. Yen, K., Lee, C., Mehta, H. & Cohen, P. The emerging role of the mitochondrial-derived peptide humanin in stress resistance. *J. Mol. Endocrinol.* **50**, R11–19. https://doi.org/10.1530/JME-12-0203 (2013).
15. Muzumdar, R. H. et al. Humanin: A novel central regulator of peripheral insulin action. *PLoS One*. **4**, e6334. https://doi.org/10.1371/journal.pone.0006334 (2009).
16. Yen, K. et al. The mitochondrial derived peptide humanin is a regulator of lifespan and healthspan. *Aging (Albany NY)* **12**, 11185–11199. https://doi.org/10.18632/aging.103534 (2020).
17. Miller, B. et al. Humanin variant P3S is associated with longevity in APOE4 carriers and resists APOE4-induced brain pathology. *Aging Cell.* **23**, e14153. https://doi.org/10.1111/acel.14153 (2024).
18. Caruso, C. & Puca, A. A. Special issue centenarians-A model to study the molecular basis of lifespan and healthspan 2.0. *Int. J. Mol. Sci.* **24**. https://doi.org/10.3390/ijms241713180 (2023).
19. Wang, X. et al. Humanin prevents high glucose-induced monocyte adhesion to endothelial cells by targeting KLF2. *Mol. Immunol.* **101**, 245–250. https://doi.org/10.1016/j.molimm.2018.07.008 (2018).
20. Hoang, P. T. et al. The neurosurvival factor Humanin inhibits beta-cell apoptosis via signal transducer and activator of transcription 3 activation and delays and ameliorates diabetes in nonobese diabetic mice. *Metabolism* **59**, 343–349. https://doi.org/10.1016/j.metabol.2009.08.001 (2010).
21. Mehta, H. H. et al. Metabolomic profile of diet-induced obesity mice in response to humanin and small humanin-like peptide 2 treatment. *Metabolomics* **15**, 88. https://doi.org/10.1007/s11306-019-1549-7 (2019).
22. Men, J., Zhang, X., Yang, Y. & Gao, D. An AD-related neuroprotector rescues transformed rat retinal ganglion cells from CoCl(2)-induced apoptosis. *J. Mol. Neurosci.* **47**, 144–149. https://doi.org/10.1007/s12031-011-9701-5 (2012).
23. Gurunathan, S., Jeyaraj, M., Kang, M. H. & Kim, J. H. Mitochondrial peptide humanin protects silver nanoparticles-induced neurotoxicity in human neuroblastoma cancer cells (SH-SY5Y). *Int. J. Mol. Sci.* **20** https://doi.org/10.3390/ijms20184439 (2019).
24. Jin, H. et al. Protective effects of [Gly14]-Humanin on beta-amyloid-induced PC12 cell death by preventing mitochondrial dysfunction. *Neurochem Int.* **56**, 417–423. https://doi.org/10.1016/j.neuint.2009.11.015 (2010).
25. Nashine, S. et al. Humanin G (HNG) protects age-related macular degeneration (AMD) transmitochondrial ARPE-19 cybrids from mitochondrial and cellular damage. *Cell. Death Dis.* **8**, e2951. https://doi.org/10.1038/cddis.2017.348 (2017).
26. Cui, A. L. et al. Humanin rescues cultured rat cortical neurons from NMDA-induced toxicity not by NMDA receptor. *ScientificWorldJournal* **2014**, 341529. https://doi.org/10.1155/2014/341529 (2014).
27. Yen, K. et al. Humanin prevents age-related cognitive decline in mice and is associated with improved cognitive age in humans. *Sci. Rep.* **8**, 14212. https://doi.org/10.1038/s41598-018-32616-7 (2018).
28. Matsunaga, D. et al. Humanin protects RPE cells from endoplasmic reticulum stress-induced apoptosis by upregulation of mitochondrial glutathione. *PLoS One* **11**, e0165150. https://doi.org/10.1371/journal.pone.0165150 (2016).
29. Minasyan, L., Sreekumar, P. G., Hinton, D. R. & Kannan, R. Protective mechanisms of the mitochondrial-derived peptide humanin in oxidative and endoplasmic reticulum stress in RPE cells. *Oxid. Med. Cell. Longev.* **2017**. 1675230. https://doi.org/10.1155/2017/1675230 (2017).
30. D'Cruz, P. M. et al. Mutation of the receptor tyrosine kinase gene Mertk in the retinal dystrophic RCS rat. *Hum. Mol. Genet.* **9**, 645–651. https://doi.org/10.1093/hmg/9.4.645 (2000).
31. Kroeger, H. et al. Induction of endoplasmic reticulum stress genes, BiP and chop, in genetic and environmental models of retinal degeneration. *Invest. Ophthalmol. Vis. Sci.* **53**, 7590–7599. https://doi.org/10.1167/iovs.12-10221 (2012).
32. Mizukoshi, S. et al. Activation of mitochondrial calpain and release of apoptosis-inducing factor from mitochondria in RCS rat retinal degeneration. *Exp. Eye Res.* **91**, 353–361. https://doi.org/10.1016/j.exer.2010.06.004 (2010).
33. Lin, B. et al. Retina organoid transplants develop photoreceptors and improve visual function in RCS rats with RPE dysfunction. *Invest. Ophthalmol. Vis. Sci.* **61**, 34. https://doi.org/10.1167/iovs.61.11.34 (2020).
34. Thomas, B. B. et al. Co-grafts of human embryonic stem cell derived retina organoids and retinal pigment epithelium for retinal reconstruction in immunodeficient retinal degenerate royal college of surgeons rats. *Front. Neurosci.* **15**, 752958. https://doi.org/10.3389/fnins.2021.752958 (2021).
35. Thomas, B. B. et al. A new immunodeficient retinal dystrophic rat model for transplantation studies using human-derived cells. *Graefes Arch. Clin. Exp. Ophthalmol.* **256**, 2113–2125. https://doi.org/10.1007/s00417-018-4134-2 (2018).
36. Zhu, Z. H., Fu, Y., Weng, C. H., Zhao, C. J. & Yin, Z. Q. Proteomic profiling of early degenerative retina of RCS rats. *Int. J. Ophthalmol.* **10**, 878–889. https://doi.org/10.18240/ijo.2017.06.08 (2017).
37. Bravo-Nuevo, A., Williams, N., Geller, S. & Stone, J. Mitochondrial deletions in normal and degenerating rat retina. *Adv. Exp. Med. Biol.* **533**, 241–248. https://doi.org/10.1007/978-1-4615-0067-4_30 (2003).
38. Seiler, M. J. et al. Vision recovery and connectivity by fetal retinal sheet transplantation in an immunodeficient retinal degenerate rat model. *Invest. Ophthalmol. Vis. Sci.* **58**, 614–630. https://doi.org/10.1167/iovs.15-19028 (2017).
39. Xin-Zhao Wang, C., Zhang, K., Aredo, B., Lu, H. & Ufret-Vincenty, R. L. Novel method for the rapid isolation of RPE cells specifically for RNA extraction and analysis. *Exp. Eye Res.* **102**, 1–9. https://doi.org/10.1016/j.exer.2012.06.003 (2012).
40. Karachaliou, C. E. & Livaniou, E. Neuroprotective action of humanin and humanin analogues: Research findings and perspectives. *Biology (Basel)* **12**. https://doi.org/10.3390/biology12121534 (2023).
41. Thiankhaw, K., Chattipakorn, K., Chattipakorn, S. C. & Chattipakorn, N. Roles of humanin and derivatives on the pathology of neurodegenerative diseases and cognition. *Biochim. Biophys. Acta Gen. Subj.* **1866**, 130097. https://doi.org/10.1016/j.bbagen.2022.130097 (2022).
42. Moin, H. et al. Effectiveness of analog of Humanin in ameliorating streptozotocin-induced diabetic nephropathy in Sprague Dawley rats. *Peptides* **165**, 171014. https://doi.org/10.1016/j.peptides.2023.171014 (2023).
43. Gultekin, F. A. et al. Effects of humanin on experimental colitis induced by 2,4,6-trinitrobenzene sulphonic acid in rats. *Saudi J. Gastroenterol.* **23**, 105–111. https://doi.org/10.4103/sjg.SJG_318_16 (2017).
44. Gottardo, M. F. et al. Antiapoptotic factor humanin is expressed in normal and tumoral pituitary cells and protects them from TNF-alpha-induced apoptosis. *PLoS One* **9**, e111548. https://doi.org/10.1371/journal.pone.0111548 (2014).
45. Zhang, X. et al. Humanin prevents intra-renal microvascular remodeling and inflammation in hypercholesterolemic ApoE deficient mice. *Life Sci.* **91**, 199–206. https://doi.org/10.1016/j.lfs.2012.07.010 (2012).
46. Rajeswaren, V. et al. Elevated tumor necrosis factor alpha and vascular endothelial growth factor in intermediate age-related macular degeneration and geographic atrophy. *Front. Ophthalmol. (Lausanne).* **4**, 1356957. https://doi.org/10.3389/fopht.2024.1356957 (2024).

47. Twarog, M. et al. TNFalpha induced by DNA-sensing in macrophage compromises retinal pigment epithelial (RPE) barrier function. *Sci. Rep.* **13**, 14451. https://doi.org/10.1038/s41598-023-41610-7 (2023).
48. Khan, A. H. et al. The effect of systemic levels of TNF-alpha and complement pathway activity on outcomes of VEGF inhibition in neovascular AMD. *Eye (Lond)* **36**, 2192–2199. https://doi.org/10.1038/s41433-021-01824-3 (2022).
49. Nassar, K. et al. Serum cytokines as biomarkers for age-related macular degeneration. *Graefes Arch. Clin. Exp. Ophthalmol.* **253**, 699–704. https://doi.org/10.1007/s00417-014-2738-8 (2015).
50. Spindler, J., Zandi, S., Pfister, I. B., Gerhardt, C. & Garweg, J. G. Cytokine profiles in the aqueous humor and serum of patients with dry and treated wet age-related macular degeneration. *PLoS One* **13**, e0203337. https://doi.org/10.1371/journal.pone.0203337 (2018).
51. Cordero-Coma, M. & Sobrin, L. Anti-tumor necrosis factor-alpha therapy in uveitis. *Surv. Ophthalmol.* **60**, 575–589. https://doi.org/10.1016/j.survophthal.2015.06.004 (2015).
52. Fernandez-Vega, B. et al. Blockade of tumor necrosis factor-alpha: A role for adalimumab in neovascular age-related macular degeneration refractory to anti-angiogenesis therapy? *Case Rep. Ophthalmol.* **7**, 154–162. https://doi.org/10.1159/000445102 (2016).
53. Theodossiadis, P. G., Liarakos, V. S., Sfikakis, P. P., Vergados, I. A. & Theodossiadis, G. P. Intravitreal administration of the anti-tumor necrosis factor agent infliximab for neovascular age-related macular degeneration. *Am. J. Ophthalmol.* **147** (830 e821), 825–830. https://doi.org/10.1016/j.ajo.2008.12.004 (2009).
54. Palczewski, K. & Kiser, P. D. Shedding new light on the generation of the visual chromophore. *Proc. Natl. Acad. Sci. USA* **117**, 19629–19638. https://doi.org/10.1073/pnas.2008211117 (2020).
55. Bocquet, B. et al. Retinitis punctata albescens and RLBP1-allied phenotypes: Phenotype-genotype correlation and natural history in the aim of gene therapy. *Ophthalmol. Sci.* **1**, 100052. https://doi.org/10.1016/j.xops.2021.100052 (2021).
56. Choi, V. W. et al. AAV-mediated RLBP1 gene therapy improves the rate of dark adaptation in Rlbp1 knockout mice. *Mol. Ther. Methods Clin. Dev.* **2**, 15022. https://doi.org/10.1038/mtm.2015.22 (2015).
57. Kvanta, A. et al. Interim safety and efficacy of gene therapy for RLBP1-associated retinal dystrophy: A phase 1/2 trial. *Nat. Commun.* **15**, 7438. https://doi.org/10.1038/s41467-024-51575-4 (2024).
58. Gorbatyuk, M. S., Starr, C. R. & Gorbatyuk, O. S. Endoplasmic reticulum stress: New insights into the pathogenesis and treatment of retinal degenerative diseases. *Prog Retin Eye Res.* **79**, 100860. https://doi.org/10.1016/j.preteyeres.2020.100860 (2020).
59. Li, H. et al. High dose expression of heme oxigenase-1 induces retinal degeneration through ER stress-related DDIT3. *Mol. Neurodegen.* **16**, 16. https://doi.org/10.1186/s13024-021-00437-4 (2021).
60. Georgiadis, A. et al. The tight junction associated signalling proteins ZO-1 and ZONAB regulate retinal pigment epithelium homeostasis in mice. *PLoS One* **5**, e15730. https://doi.org/10.1371/journal.pone.0015730 (2010).
61. Zhou, M. et al. Role of Epithelial-mesenchymal transition in retinal pigment epithelium dysfunction. *Front. Cell. Dev. Biol.* **8**, 501. https://doi.org/10.3389/fcell.2020.00501 (2020).
62. Zheng, Y. & Chen, S. Transcriptional precision in photoreceptor development and diseases - Lessons from 25 years of CRX research. *Front. Cell. Neurosci.* **18**, 1347436. https://doi.org/10.3389/fncel.2024.1347436 (2024).
63. Langouet, M. et al. Mutations in BCOR, a co-repressor of CRX/OTX2, are associated with early-onset retinal degeneration. *Sci. Adv.* **8**, eabh2868. https://doi.org/10.1126/sciadv.abh2868 (2022).
64. Pan, D., Zhang, X., Jin, K. & Jin, Z. B. CRX haploinsufficiency compromises photoreceptor precursor translocation and differentiation in human retinal organoids. *Stem Cell. Res. Ther.* **14**, 346. https://doi.org/10.1186/s13287-023-03590-3 (2023).
65. Avery, S. et al. BCL-XL mediates the strong selective advantage of a 20q11.21 amplification commonly found in human embryonic stem cell cultures. *Stem Cell. Rep.* **1**, 379–386. https://doi.org/10.1016/j.stemcr.2013.10.005 (2013).
66. Chong, S. J. F. et al. Noncanonical Cell Fate Regulation by Bcl-2 Proteins. *Trends Cell. Biol.* **30**, 537–555. https://doi.org/10.1016/j.tcb.2020.03.004 (2020).
67. Abbasalizadeh, S. & Baharvand, H. Technological progress and challenges towards cGMP manufacturing of human pluripotent stem cells based therapeutic products for allogeneic and autologous cell therapies. *Biotechnol. Adv.* **31**, 1600–1623. https://doi.org/10.1016/j.biotechadv.2013.08.009 (2013).
68. Zhang, N. et al. The importance of Bcl-xL in the survival of human RPE cells. *Invest. Ophthalmol. Vis. Sci.* **48**, 3846–3853. https://doi.org/10.1167/iovs.06-1145 (2007).
69. Lee, K. S., Lin, S., Copland, D. A., Dick, A. D. & Liu, J. Cellular senescence in the aging retina and developments of senotherapies for age-related macular degeneration. *J. Neuroinflamm.* **18**, 32. https://doi.org/10.1186/s12974-021-02088-0 (2021).
70. Ryu, W., Park, C. W., Kim, J., Lee, H. & Chung, H. The Bcl-2/Bcl-xL Inhibitor ABT-263 attenuates retinal degeneration by selectively inducing apoptosis in senescent retinal pigment epithelial cells. *Mol. Cells* **46**, 420–429. https://doi.org/10.14348/molcells.2023.2188 (2023).
71. DeGregori, J. & Johnson, D. G. Distinct and overlapping roles for E2F family members in transcription, proliferation and apoptosis. *Curr. Mol. Med.* **6**, 739–748. https://doi.org/10.2174/1566524010606070739 (2006).
72. Putzer, B. M. & Engelmann, D. E2F1 apoptosis counterattacked: Evil strikes back. *Trends Mol. Med.* **19**, 89–98. https://doi.org/10.1016/j.molmed.2012.10.009 (2013).
73. Klein, R. et al. Markers of inflammation, oxidative stress, and endothelial dysfunction and the 20-year cumulative incidence of early age-related macular degeneration: The Beaver Dam Eye Study. *JAMA Ophthalmol.* **132**, 446–455. https://doi.org/10.1001/jamaophthalmol.2013.7671 (2014).
74. Gong, C. et al. IL-6-induced acetylation of E2F1 aggravates oxidative damage of retinal pigment epithelial cell line. *Exp. Eye Res.* **200**, 108219. https://doi.org/10.1016/j.exer.2020.108219 (2020).
75. Miller, A. F. Superoxide dismutases: Ancient enzymes and new insights. *FEBS Lett.* **586**, 585–595. https://doi.org/10.1016/j.febslet.2011.10.048 (2012).
76. Zelko, I. N., Mariani, T. J. & Folz, R. J. Superoxide dismutase multigene family: A comparison of the CuZn-SOD (SOD1), Mn-SOD (SOD2), and EC-SOD (SOD3) gene structures, evolution, and expression. *Free Radic Biol. Med.* **33**, 337–349. https://doi.org/10.1016/s0891-5849(02)00905-x (2002).
77. Mueller-Buehl, A. M. et al. Reduced retinal degeneration in an oxidative stress organ culture model through an iNOS-inhibitor. *Biology (Basel)* **10** https://doi.org/10.3390/biology10050383 (2021).
78. Owji, A. P., Kittredge, A., Zhang, Y. & Yang, T. Structure and function of the bestrophin family of calcium-activated chloride channels. *Channels (Austin)* **15**, 604–623. https://doi.org/10.1080/19336950.2021.1981625 (2021).
79. Kong, M. D. et al. Divergent manifestations in biallelic versus monoallelic variants of RP1-, BEST1-, and PROM1-associated retinal disorders. *Int. J. Mol. Sci.* **26** https://doi.org/10.3390/ijms26146615 (2025).
80. Karaosmanoglu, B., Imren, G., Utine, E., Taylan Sekeroglu, H. & Taskiran, E. Z. Allele-specific antisense oligonucleotides for the treatment of BEST1-related dominantly inherited retinal diseases: An in vitro model. *Exp. Eye Res.* **241**, 109833. https://doi.org/10.1016/j.exer.2024.109833 (2024).

Acknowledgements

The authors want to acknowledge the contribution of Dr. M.C. Kenney, UCI (who passed away in December 2023) to the initiation, funding and completion of this project. The authors would like to acknowledge the technical assistance of Shari R. Atilano, Mithalesh Singh (Kenney lab), and Seiler lab staff members Robert Sims,

Karla Echeverria, Jay Santoso, Reeva Reyes, Jeffrey Delgado; and students Alice Avetyan, Candice Wu, Caroline Lee, Jennie Xu, Kevin Wu, Angel Blanquel, Adeline Cheng, Winnie Luong, Julianne Frances Agapinan, Ceci Zhang, Ani Petrosyan, Ani Khachigian, Ryan Pavey. Christopher Quimpo, Maihan Phan, and other students. This research was funded by the National Eye Institute, grant R01 EY027363 and to a small part with grant R01 EY031834. The authors acknowledge support to the Gavin Herbert Eye Institute at the University of California, Irvine from an unrestricted grant from Research to Prevent Blindness and from NIH core grant P30 EY034070.

Author contributions

BL: performed experiments, collected & analyzed data; wrote the paper; edited figures; approved the final versionKS: performed experiments, collected & analyzed data; wrote the paper; approved the final versionMO: performed experiments, collected & analyzed data; wrote the paper; approved the final versionNI: performed experiments, collected data; approved the final versionMJS: performed experiments, analyzed data; wrote the paper; edited figures; provided funding; approved the final version.

Funding

This research was funded by the National Eye Institute, grant R01 EY027363 and to a small part with grant R01 EY031834. The authors acknowledge support to the Gavin Herbert Eye Institute at the University of California, Irvine from an unrestricted grant from Research to Prevent Blindness and from NIH core grant P30 EY034070.

Declarations

Competing interests

The authors declare no competing interests.

Additional information

Supplementary Information The online version contains supplementary material available at https://doi.org/10.1038/s41598-026-62834-3.

Correspondence and requests for materials should be addressed to M.J.S.

Reprints and permissions information is available at www.nature.com/reprints.

Publisher's note Springer Nature remains neutral with regard to jurisdictional claims in published maps and institutional affiliations.

Open Access This article is licensed under a Creative Commons Attribution 4.0 International License, which permits use, sharing, adaptation, distribution and reproduction in any medium or format, as long as you give appropriate credit to the original author(s) and the source, provide a link to the Creative Commons licence, and indicate if changes were made. The images or other third party material in this article are included in the article's Creative Commons licence, unless indicated otherwise in a credit line to the material. If material is not included in the article's Creative Commons licence and your intended use is not permitted by statutory regulation or exceeds the permitted use, you will need to obtain permission directly from the copyright holder. To view a copy of this licence, visit http://creativecommons.org/licenses/by/4.0/.

© The Author(s) 2026